Molecular Diffusion in Hierarchical Zeolites with Ordered Mesoporosity: Pulsed Field Gradient Nuclear Magnetic Resonance Combined with Thermodynamic Modeling

S. Dutta, A. Galarneau, D. Minoux, C. Aquino, J. Dath, Flavien Guenneau, B. Coasne

Molecular Diffusion in Hierarchical Zeolites with Ordered Mesoporosity: Pulsed Field Gradient Nuclear Magnetic Resonance combined with Thermodynamic Modeling

S. Dutta,[‖] A. Galarneau,[†,*] D. Minoux,[‡] C. Aquino, [‡]

J. P. Dath,[‡] F. Guenneau,[‖,*] B. Coasne[§,*]

[‖] Sorbonne Université, CNRS, Laboratoire de Chimie de la Matière Condensée de Paris, LCMCP, 75252 Paris, France

[†] Institut Charles Gerhardt Montpellier, Univ. Montpellier, Balard Recherche, Pôle Chimie, ICGM UMR 5253, 1919 Rte de Mende, 34293 Montpellier Cedex 5, France

[‡] Total Energies One Tech Belgium, Zone industrielle C, 7181 Feluy, Belgium

[§] Univ. Grenoble Alpes, CNRS, LIPhy, 140 rue de la Physique – Domaine Universitaire BP 87 – 38402 Saint Martin d'Heres Cedex, France

TOC Graphic

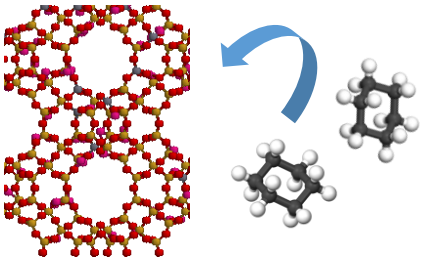

* To whom correspondence should be addressed: Anne Galarneau (anne.galarneau@enscm.fr), Flavien Guenneau (flavien.guenneau@sorbonne-universite.fr), Benoit Coasne (benoit.coasne@univ-grenoble-alpes.fr)

ABSTRACT: The dynamics of fluids confined in hierarchical porous materials, is gaining increasing attention. Here, using Pulsed Field Gradient Nuclear Magnetic Resonance, we report an experimental study of the self-diffusivity of cyclohexane confined at different temperatures in the bi-porous structure of hierarchical faujasite zeolites (i.e. combining the intrinsic zeolite microporosity < 2 nm and an ordered MCM-41 like mesoporosity of 4 nm diameter). For different mesoporous volumes, we consider cyclohexane self-diffusivity at chemical potentials where the porosity is either totally or only partially filled (in the latter case, the microporosity is completely filled while the mesopore surface is only covered by a molecular thin film). On one hand, in completely filled materials, as expected, the effective cyclohexane self-diffusivity is found to increase as the mesoporous volume increases. Moreover, in this regime, the self-diffusivity follows an Arrhenius behavior with an activation energy that is close – although slightly smaller – than that for bulk cyclohexane. On the other hand, for partially filled materials, a striking behavior is observed as the measured self-diffusivity decreases upon increasing the loading and remains nearly constant upon increasing the temperature. We propose here that such behavior can be rationalized by considering (1) the population redistribution between the microporosity and mesoporosity (including the gas phase in the mesopores) and (2) the effective number of molecules that contributes to spin echo attenuation upon increasing the temperature. In particular, while molecules diffuse overall faster with increasing the temperature, we show here that our measurements rely at each temperature on a slower and slower population (therefore leading to unexpected temperature variations).

1. INTRODUCTION

Owing to their large surface area (~10^2 – 10^3 m^2/g) and regular pore size (~ nm), zeolites are porous crystalline materials with optimal properties for catalysis, adsorption, ion-exchange, etc.[1] To alleviate mass transfer limitations in their very small porosity, much effort is still being devoted to synthesize multiscale porous zeolites exhibiting different porosity scales – the so-called hierarchical zeolites, micro/mesoporous materials and/or biporous zeolites.[2,3,4,5,6] All these different systems refer to the same type of porous samples, which combine the zeolite microporosity (< 2 nm) hosting the active surface sites and a mesoporous network (2 – 50 nm) ensuring fast and unrestricted access to these active sites. Yet, despite many similar properties, the different design strategies that lead to such multiscale zeolites confer them with different properties. In particular, the dynamics and transport of confined fluids is known to be very sensitive to the pore size, distribution, and connectivity of the micro- and mesoporous domains. Typically, poor connectivity between the microporous/mesoporous domains or buried mesoporosity accessible from micropores only lead to very little improvement with respect to the reference, i.e. only microporous, zeolite.

The complexity in describing and predicting transport in multiscale porous materials drastically hinders the development of rational design strategies of hierarchical zeolites. In particular, despite the recent research boost in the synthesis of more and more hierarchical zeolites, the on demand design of optimal samples for a given application is still out of reach. To attain this goal, in parallel to synthesis efforts and advancements in adsorption kinetics modelling,[7,8] significant research has been devoted to the development of robust experimental procedures to assess transport and diffusion in such multiscale porous materials.[9,10] In particular, as an alternative to in-flow experiments which probe transport in conditions close to real applications, microscopic diffusion experiments such as quasi elastic neutron scattering (QENS[11,12]), nuclear magnetic resonance diffusometry (NMR relaxometry[13,1415]) and pulsed field gradient nuclear magnetic resonance (PFG NMR[16,17,18]) are receiving a lot of attention. With such experiments, one simplifies the problem by restricting the investigation of transport phenomena to self-diffusion (i.e., no net flow conditions). Even though the self-diffusivity provides an incomplete picture of in-flow transport in porous materials, it is often found to be very valuable and sufficient as it corresponds to the main contribution in the collective diffusivity (which is linked to the permeance in transport induced by a pressure gradient)[19]. This is particularly true for gas transport and/or ultraconfined molecules where the velocity

correlations between different molecules are very small or even negligible.[20] Among the different techniques available to probe self-diffusion, PFG NMR is considered a method of choice as it probes transport over time and length scales that involve diffusion across multiple porosity domains or restricted to given porosity domains. In more detail, depending on the experimental conditions used (temperature, observation time, field gradient range, loading, etc.), diffusion is assessed with many molecules crossing back and forth different domain types or with most molecules confined within the same porosity domain types.[17,18,21]

Here, we report an experimental study using PFG NMR on the self-diffusion of cyclohexane confined at different temperatures in the hierarchical porosity of micro/mesoporous faujasite zeolites. The samples consist of NaY faujasite zeolites (Si/Al = 15) in which an ordered MCM-41 type mesoporosity is formed using an octadecyltrimethylammonium surfactant (C18 chain) so that the typical mesopore diameter is about 4 nm.[24] Different mesoporous volumes are considered in order to probe the effect of this parameter on cyclohexane self-diffusivity. Moreover, to assess the underlying diffusion mechanisms, different loadings are considered with the whole porosity being either completely or only partially filled. In addition to shedding light on the diffusion of this probe in hierarchical materials, the present study shows some important difficulties inherent to the PFG NMR technique. In particular, by carefully analyzing the change in the fraction of molecules probed upon increasing the temperature, it is illustrated how counterintuitive results such as nearly constant temperature dependence of self-diffusion can be explained.

2. SAMPLES AND METHODS

2.1. Materials

In a beaker (250 mL), NaOH pellets were added to 180 g of H_2O and the mixture was stirred with a magnet until complete dissolution at 25°C. Then, 7.843 g of octadecyltrimethylammonium bromide (C18TAB) was added under magnetic stirring until complete dissolution at 25°C. In this regard, different masses of NaOH pellets were used to achieve the respective zeolite compositions (for the compositions see Table S1, Supporting Information). The magnetic stirrer was then replaced by an endless screw stirrer, which provides a gentler stirring that is necessary to maintain the particle size and shape of the initial

material, as described for the pseudomorphic synthesis of silica particles into MCM-41 particles.[22,23] Indeed, the present synthesis relies on the concept of pseudomorphic transformation but with zeolites as starting materials instead of silica or silica-alumina. Next, approximately 12 g of the parent zeolite, i.e., dealuminated H^+-FAU-Y (Si/Al = 15) (CBV720, obtained from Zeolyst) was added to the solution and stirred for 1–2 h at 25°C until a homogeneous white suspension was obtained. The suspension was then transferred into a Teflon-lined stainless steel autoclave (250 mL) and maintained in a static condition for 20 h at 115°C. It was then filtered and washed with water until neutral pH was reached. The sample was then dried in an oven at 80°C for 12 h and calcined at 550°C for 8 h (heating rate 5 K/min). The molar ratios of the mixtures were calculated by approximating the FAU-Y composition as 1 SiO_2: 0.1 C18TAB: *n* NaOH: 50 H_2O, where *n* = 0.025 to 0.25.[24]

2.2. Characterization techniques

The structural characterization of the mesoporous faujasites was conducted by X-ray diffraction (XRD) using a Bruker D8 Advance diffractometer with a Bragg-Brentano geometry. The diffractometer emitted Cu Kα radiation and was equipped with a Bruker Lynx Eye detector and a Ni filter. The XRD patterns were recorded in the 2θ range of 4–50° to identify the peaks corresponding to FAU-Y, and in the range of 0.04–6° to identify the ordering of the mesopores.[24] The textural properties of the mesoporous faujasites were determined by N_2 sorption isotherms at 77 K, recorded on a Belsorb apparatus. Prior to this characterization, approximately 200–300 mg of the sample that was used for analysis was outgassed under vacuum at 250°C for 12 h. The Broekhoff and De Boer (BdB) method was applied to the N_2 desorption isotherm to calculate the mesopore diameters – as recommended for MCM-41 type materials.[25] The micro-, meso-, and total pore volumes were evaluated by the corrected t-plot method developed previously for mesoporous FAU-Y[28] and recently extended to various hierarchical zeolites.[26] The transmission electron microscopy (TEM) images were recorded using a JEOL 1200 EX2 microscope operating at 100 kV.

2.3. Pulsed Field Gradient Nuclear Magnetic Resonance

Cyclohexane was loaded in the sample by freezing the desired amount of material (between 40–100% of the total pore volume) inside the NMR tube, which was then sealed and left at

room temperature for at least 48 h prior to the experiments. The measurements of self-diffusion coefficients of cyclohexane were performed on an Avance HD Bruker spectrometer operating at a ^{1}H resonance frequency of 300 MHz. Pulsed field gradients were generated by a Bruker diffusion probe equipped with a Diff50 gradient coil connected to a Great60 DC current amplifier, leading to a maximum attainable gradient of 30 T m^{-1}. Since the transverse relaxation time, T_2, of cyclohexane adsorbed in our materials was typically on the order of 1 ms or less, short 370 μs gradient pulses were used and the gradient intensity was varied between 10–1500 G/cm. A stimulated echo sequence was used to take advantage of the long longitudinal relaxation time, T_1 (compared to the transverse relaxation time T_2). Additionally, to avoid the influence of internal magnetic field gradients on the attenuation of the echo signal, the bipolar gradient variant proposed by Cotts et al.[27] (named the 13-interval pulse sequence) was chosen. The observation time, Δ, was varied between 10–80 ms for preliminary experiments and subsequently set to 10 ms for the whole set of measurements. Given the large number of samples under consideration and the long duration of each PFG NMR experiment, it was possible to perform a complete diffusion measurement for only selected nanoporous samples, i.e., obtaining the NMR signal attenuation as a function of magnetic field gradient for both complete/partial loading at all temperatures. Therefore, a selection of samples, temperatures and loadings was made to gain insights into the impact of temperature and loading as a function of the mesoporosity/mesoporous volume in the mesoporous faujasites.

3. MATERIALS CHARACTERIZATION

The parent FAU-Y is made up of particles with a typical diameter of ~10 μm (2 – 20 μm). Such particles are formed by the aggregation of crystals of size ~1 μm. On the other hand, the mesoporous FAU, which result from the pseudomorphic transformation of FAU-Y assisted by C18TAB, is composed of particles of diameter ~20 μm (10 – 90 μm) formed by the aggregation of crystals of size ~1 μm. As shown in Fig. 1, mesoporous FAU materials correspond to two main classes of hierarchical micro/mesoporous materials. (Type 1) For 0.0625 < NaOH/Si < 0.10, the walls in between ordered mesopores are presumably zeolitic as the wall thickness (2.4 nm) is large enough to accommodate the FAU unit cell. Another variant of such materials also contain some zeolite nanocrystals (100 – 200 nm) well-dispersed in each grain. (Type 2) For 0.125 < NaOH/Si < 0.25, the walls in between mesopores are presumably amorphous as the wall thickness (1 nm) is too small to

accommodate a FAU unit cell. In each grain some well-dispersed zeolite nanocrystals are present, the size of which decreases with the increase of NaOH/Si ratio (from 100 to 4 nm). Within the grains, some macropores form as well, the diameter and number of which increase with the NaOH/Si ratio.[24] Using the *t*-plot analysis (Table S1 in the Supporting Information) applied to nitrogen sorption at 77 K (Fig. 2), it was shown that increasing the NaOH/Si ratio from 0.025 to 0.25 increases the mesoporous volume from ~0 to 0.75 mL/g, while decreasing the microporous volume from ~0.37 to 0.06 mL/g. The mesopore diameters are ~4.4 nm for 0.06 < NaOH/Si < 0.1, respectively, and decrease linearly with increasing NaOH/Si (0.125 < NaOH/Si < 0.25) to reach ~4.0 nm (Fig. 2). The mesopore diameter distribution is narrow: ± 0.3 nm for 0.06 < NaOH/Si < 0.1 and ± 0.5 nm for 0.125 < NaOH/Si < 0.25. The micropore sizes are defined by the zeolite structure of FAU determined from XRD[24] with windows and cavities of 0.78 nm and 1.3 nm, respectively. On the one hand, the microporous surface area decreases from 800 to 0 m^2/g upon increasing NaOH/Si from 0.025 to 0.25, on the other hand, the mesoporous surface area increases from 30 to 800 m^2/g. The external surface area is ~30 m^2/g for 0.075 < NaOH/Si < 0.25, being ~100 m^2/g for the parent FAU-Y and untransformed zeolite for 0 < NaOH/Si < 0.05.[28,29] The micro- and mesoporous volumes of the mesoporous FAU-Y (based on the NaOH/Si ratios) have been referred from values previously reported by Mehlhorn et. Al, [24] as listed in table 1. Based on the work of Reich et al[30], the mesoporosities of individual zeolite samples were calculated from the mesoporous volume (V_m), total porous volume (V_{tot}), and density of the solid skeleton of the respective zeolites and are listed in Table 1.

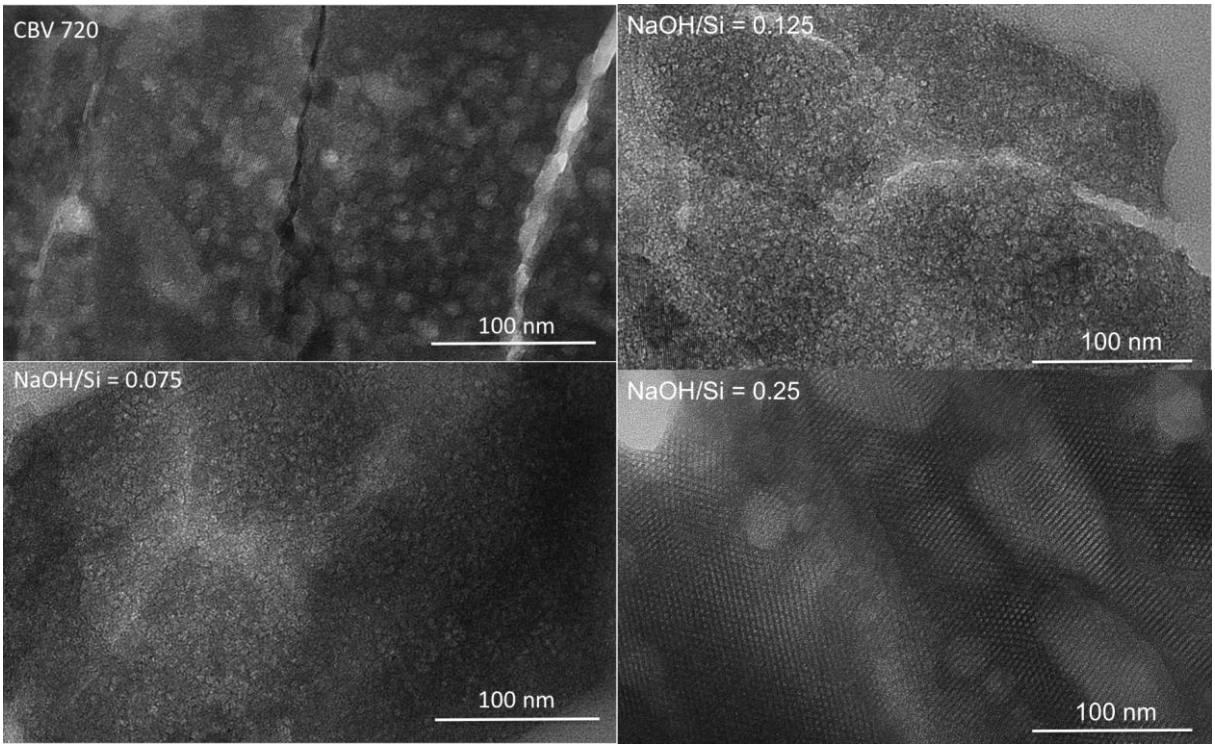

Fig. 1. Transmission electron microscopy images of the starting zeolite (FAU-Y, named CBV 720) and of the mesoporous FAU exhibiting mesoporosity obtained using different NaOH/Si molar ratios: NaOH/Si 0.075, 0.125, 0.25. The scale is shown on each image. The dark regions show the pore walls while the light regions show the pore voids.

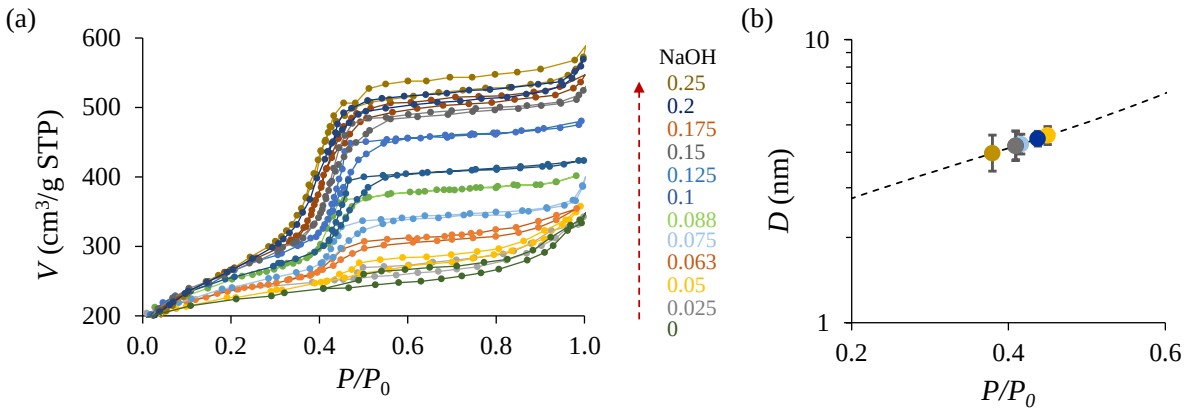

Fig. 2. (a) Nitrogen sorption isotherms at 77 K of mesoporous FAU obtained using different NaOH/Si molar ratios ranging from 0–0.25. The adsorbed amounts V are expressed in cm^3 STP per g of solid material as a function of the relative pressure P/P_0 (P_0 is the bulk saturating vapor pressure for N_2 at 77 K). The NaOH/Si molar ratio is shown on the right. Starting from NaOH/Si = 0 (regular zeolite), the mesoporosity inside the mesoporous FAU increases with the NaOH/Si molar ratio (as evidenced by both the increase in the adsorbed amount prior to capillary condensation and the sharp increase in the adsorbed amount corresponding to capillary condensation). (b) Pore size, D, versus capillary condensation pressure as obtained using the Broekhoff and De Boer (BdB) (desorption curve) relationship. The dashed line is the analytical relationship while the filled circles correspond to the mesoporous FAU for which the N_2 adsorption isotherms are shown in panel (a) with the same color code. The extracted mesoporous diameters, D, are also shown for each mesoporous FAU in Table 1.

Table 1: Average mesopore diameter, microporous, mesoporous and total pore volumes of the mesoporous FAU obtained from N_2 sorption isotherms at 77 K.[24] Additionally, the mesoporosities, ε, are also listed (these values have been calculated based on the work of Reich et al.[38])

NaOH/Si	*D* *(nm)*	V_{tot} (mL/g)	V_{μ} (mL/g)	V_m (mL/g)	ϵ (mesoporosity)
0		0.431	0.371	0.06	0.06
0.05	4.58	0.437	0.326	0.111	0.12
0.075	4.27	0.534	0.28	0.254	0.24
0.10	4.46	0.634	0.222	0.411	0.36
0.125	4.21	0.714	0.17	0.544	0.44
0.15	4.21	0.766	0.122	0.644	0.50
0.25	3.97	0.811	0.057	0.754	0.57

4. DIFFUSION

While PFG NMR is a robust and successful technique to probe transport in micro/mesoporous materials, such as hierarchical zeolites, data interpretation is often very complex as it depends on the specificities of the porous solid and adsorbed fluid as well as on the thermodynamic and acquisition conditions.[31,32] Typically, for the same porous sample, depending on the fluid probe and observation time, Δ, considered, the interpretation of the diffusion data will greatly differ. In principle, this is an asset of the PFG NMR technique as the use of different fluids (or temperatures) and observation times allows probing either diffusion restricted to molecules that do not exchange between porosity domains or macroscopic diffusion with molecules that explore all porosity domains.[18,31,32] In more detail, in the first case, the exchange time, τ, between domains is much longer than the observation time, Δ, such that the PFG NMR data shows different diffusion regimes that are characteristic of each porosity domain (micro-, meso-, and macroporous). In contrast, in the second case, the exchange time, τ, between domains is shorter than the observation time, Δ, such that the PFG NMR data shows a single diffusion regime that is characteristic of the whole porous material and its underlying distribution of micro-, meso-, and macroporous domains. Therefore, by playing with Δ (which can be tuned between a few ms to a few hundreds of ms typically), one can probe in principle surface barriers through the corresponding characteristic crossing time, τ, that they induce. However, despite its robustness and efficiency, the difficulty and variability of the interpretation of PFG NMR data often lead to confusing pictures when multiscale porous materials are used. In fact, this complexity arises from the dual nature of the PFG NMR technique which probes diffusion over both, a given time and length scale, respectively; wherein Δ sets a characteristic time, and the magnetic field gradient imposes a spatial length, ξ.

In practice, with the PFG NMR technique, the diffusion coefficient is obtained from the attenuation, Ψ, of the PFG NMR echo signal measured as a function of the amplitude of the applied field gradient, g. The dependence of Ψ on the experimental parameters in the case of diffusion in an infinite homogeneous medium is expected to take the form: $\Psi = exp\left[-\gamma^2\delta^2 g^2 D_{eff}\Delta\right]$. γ is the gyromagnetic ratio of the observed nucleus, δ is the duration of the gradient pulses, and, Δ, the effective observation time, includes corrections arising from the particular pulse sequence used. The representation of Ψ in logarithmic scale

versus $q = \gamma^2\delta^2 g^2 D_{eff}\Delta$ should therefore lead to a straight line and, D_{eff}, the effective diffusion coefficient (m^2 s^{-1}) to be measured is usually obtained by fitting the experimental data against the above equation. However, all our data exhibit a more complex dependence consisting of two distinct parts: a rapid decrease at very low values of the magnetic field gradient followed by a straight line with a slight negative slope (Fig. 3(a)). The rapid decrease, corresponding to large molecular displacements (long range diffusion), is due to the fraction of molecules that exchange at some point between intraparticle and interparticle spaces during the observation time. The second part of the curve with much smaller slope corresponds to the molecules diffusing inside the particles only and moving over smaller distances during the same observation time. The fitting of that part gives the value of the diffusion coefficient inside the hierarchical particles, whereas the extrapolation of the linear part to the vertical axis leads to an approximation of the proportion of molecules considered. As observed in Fig. 3(b), the diffusion coefficient is almost independent of Δ up to a value of 60 ms, after which it starts to decrease drastically as a consequence of a transport resistance at the surface of the particles. As the diffusion time is increased, the mean displacement of the molecules increases and more of them are able to leave the particles. Some of the molecules that encounter the surface of the particles cannot overcome the energy barrier to leave the porous network and get reflected inside. The mean displacement of the observed set of molecules is therefore decreased and the measured D_{eff} depends on Δ (restricted diffusion). Consequently, it was decided to use Δ = 10 ms in order to avoid any bias coming from this phenomenon on our measurements.

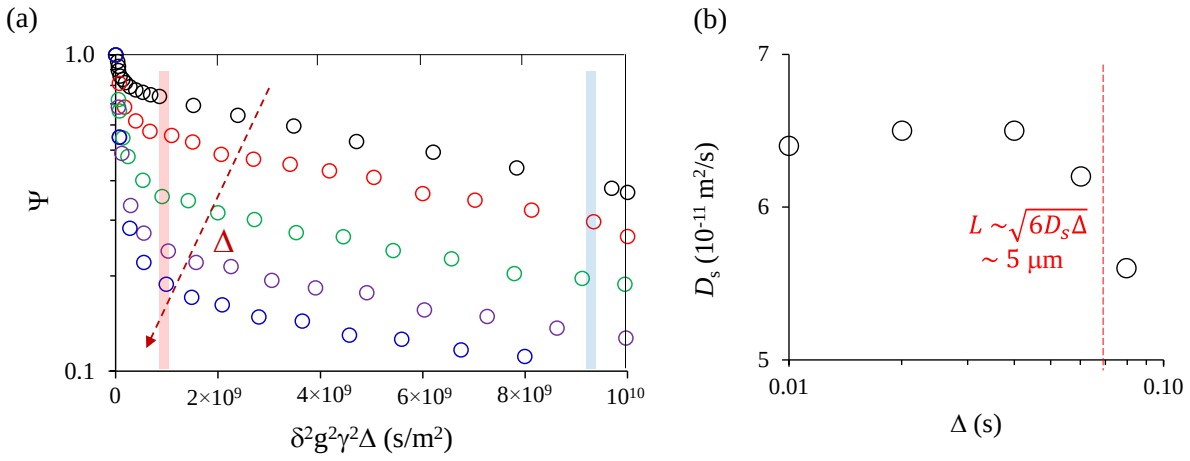

Fig. 3. (a) Attenuation Ψ of the spin echo signal at -20°C as a function of the gradient strength, g, measured from PFG NMR for cyclohexane adsorbed in a mesoporous FAU (the NaOH/Si molar ratio is 0.25). The porosity is filled up to 100%, which means that both the microporosity and mesoporosity are filled with cyclohexane (*see text*). These measurements were performed for different observation times, Δ: (black) 10 ms, (red) 20 ms, (green) 40 ms, (purple) 60 ms, and (blue) 80 ms. Considering the observation times, these measurements correspond to molecules with typical displacements $L \sim (6D_s\Delta)^{1/2}$. This corresponds to L in the range 1 – 3 μm for Δ = 10 ms, and L in the range 3 – 9 μm for Δ = 80 ms. (b) Self-diffusivity, D_s, as a function of Δ for cyclohexane obtained from the fit of the spin echo attenuation curves in (a). For Δ < 60 ms, the self-diffusivity corresponds to the molecules that remain within the mesoporous FAU particles as PFG NMR probes displacements L < 1.5 μm, i.e., smaller than the particle radius. In contrast, for Δ > 60 ms, the self-diffusivity drops as PFG NMR probes displacements that extend beyond the particles size so that diffusion is sensitive to energy barriers at the particle surface.

4.1. Complete pore filling

We first discuss the results obtained upon complete pore filling for the series of mesoporous FAU. Fig. 4(a) shows the self-diffusivity obtained using PFG NMR for cyclohexane at T = -20 °C in these porous solids as a function of the mesoporous volume (the corresponding attenuation curves are shown in Fig. S1 of the Supporting Information). For the sake of clarity, we also report in Fig. 4(a) the corresponding NaOH/Si molar ratio used to prepare each sample and the resulting mesoporosity. As expected, upon increasing the mesoporous volume available in the sample, the effective diffusivity, D_s, increases; under such complete filling conditions, molecules exchange between the microporous and mesoporous domains such that the effective diffusivity probed by PFG NMR reflects an average diffusivity of the micro- and mesoporous domains combined. To further assess the correlation between the properties of each prepared material and these experimental diffusion data, we show in Fig. S2 (Supporting Information) the same self-diffusion data plotted as a function of the other physical parameters, i.e., the mesopore size, D, the mesoporosity, ε, and the NaOH content used in the synthesis [note that the abscissae in Fig. 4(a) is the mesoporous volume V_m]. As expected, the mesopore diameter is found to be non-relevant as the different samples have

very similar diameters. This finding is confirmed by the fact that the self-diffusivity for the pure zeolite, despite the absence of mesoporosity, has the same order of magnitude as that for the mesoporous FAU materials. We found that D_s for the mesoporous FAU is strongly correlated with the mesoporosity, ε, and the NaOH content used in the synthesis. The marked correlation with ε was expected as this parameter is directly related to the mesoporous volume V_m so that the dependence $D_s(\varepsilon)$ is intrinsically linked to $D_s(V_m)$. Similarly, the correlation observed between D_s and [NaOH/Si] is also expected as the latter parameter directly impacts V_m (in fact, [NaOH/Si] is the driving force to form mesoporosity in the faujasite samples). However, in this case, we note that there is no trivial, i.e., mathematical dependence between V_m and [NaOH/Si], and the similar trends observed in $D_s(V_m)$ and D_s([NaOH/Si]) are only qualitative.

The data in Fig. 4(a) can be rationalized by invoking the self-correlation function $G(r,t) \sim [D_s t]^{-1/2} \exp[-r^2/D_s t]$ which describes the probability that a cyclohexane molecule diffuses by a distance r over a time t (note that the use of a Gaussian distribution implicitly assumes that the displacement obeys normal, i.e. Fickian diffusion). This function or equivalently its space Fourier transform (where $r = q^{-1}$), $I(q,t) \sim \exp[-D_s q^2 t]$, contains all information on the dynamics within each porous domain but also on the crossing dynamics between domains. From a general point of view, such crossing dynamics lead to complex functions $I(q,t)$, such that the effective diffusivity, D_s^{eff}, cannot be predicted in a straigthforward fashion from the self-diffusivities in the purely microporous and mesoporous domains (D_s^{μ} and D_s^{m}). However, there are two asymptotic regimes where diffusion can be described accurately in a very simple manner. Let us consider the diffusion time, t, is $\tau_D^k \sim (D_s^k q^2)^{-1}$ to diffuse over a typical length $L \sim 1/q$ in a domain k. On the one hand, when the typical crossing time τ_C is such that $\tau_D^k << \tau_C$, most molecules remain in the same domain and $I(q,t)$ in this slow-switching limit is given by the sum of all intra-domain diffusion components: $I(q,t) = \Sigma_k x_k \exp[-D_s^k q^2 t]$ where x_k is the fraction of molecules located in the porous domains of type k. On the other hand, when the crossing time τ_C is such that $\tau_D^k >> \tau_C$, molecules do exchange frequently between domain types and $I(q,t)$ in this fast-switching limit corresponds to a single exponential component $I(q,t) = \exp[-D_s^{eff} q^2 t]$ with an effective diffusivity given by D_s^{eff}. In practice, the expression for D_s^{eff} can be rather complex as it depends on the way the domains are distributed but also on the specificities of the interfaces

between them (existence of surface diffusion barriers, crossing/recrossing properties, etc.). However, there is a simple approximation – known as fast exchange model[31,32] – that can be made to derive the following expression for the effective self-diffusivity $D_s^{eff} = \Sigma_k x_k D_s^k$. This last result can be derived in a simple fashion as follows. In the Fickian regime, D_s^{eff} is linked to the average mean square displacement:[9,18]

$$\langle r^2 \rangle = \langle \left(\sum_k \sum_i \Delta \mathbf{r}_k^i \right)^2 \rangle \sim \sum_k \sum_i \langle (\Delta \mathbf{r}_k^i)^2 \rangle \qquad (1)$$

where $\Delta \mathbf{r}_k^i$ is the i^{th} trajectory segment within a domain of type k and < > denotes statistical averaging. In the second equation, all successive trajectory segments were assumed to be uncorrelated i.e. $< \Delta \mathbf{r}_k^i \Delta \mathbf{r}_{k'}^{i'} > = 0$ (except if $i = i'$ and $k = k'$). Furthermore, upon assuming that each trajectory obeys Fickian diffusion, i.e. $(\Delta \mathbf{r}_k^i)^2 = 6 D_s^k t$, Eq. (1) can be recast as $\langle r^2 \rangle = 6 D_s^{\text{eff}} t$ with:

$$D_s^{\text{eff}} = \sum_k t_k D_s^k = \sum_k x_k D_s^k \qquad (2)$$

where t_k is the time fraction spent in domains of type k. In the second equality in Eq. (2), the ergodicity principle was used to convert the time fraction t_k into the average molecular population fraction x_k in domains of type k.

Coming back to our experimental data shown in Fig. 4(a), the underlying spin echo attenuation data suggest that after the initial fast decay only one diffusion constant is observed in the range corresponding to microporous and mesoporous diffusion. In turn, this suggests that diffusion in the hierarchical samples considered here involves an effective diffusivity D_s^{eff} as defined by Eq. (2). This result is supported by the fact that experimental data in Fig. 4(a) are reasonably well described using Eq. (2) (see the dashed line in the figure). The fitted microporous and mesoporous self-diffusion coefficients were found to be $D_s^{\mu} \sim 2.5 \times 10^{-11}$ and $D_s^{m} \sim 5.6 \times 10^{-11}$ m^2/s, respectively. It should be emphasized that these values do not necessarily reflect the true self-diffusivity as would be encountered in purely ideal microporous and mesoporous phases. Indeed, they should rather be seen as mesoscopic values – probed for diffusion over the micron scale – which include the effect of tortuosity and defects within the corresponding microporosity and mesoporosity (in fact, self-diffusion coefficients within such phases are expected to differ by at least an order of magnitude).

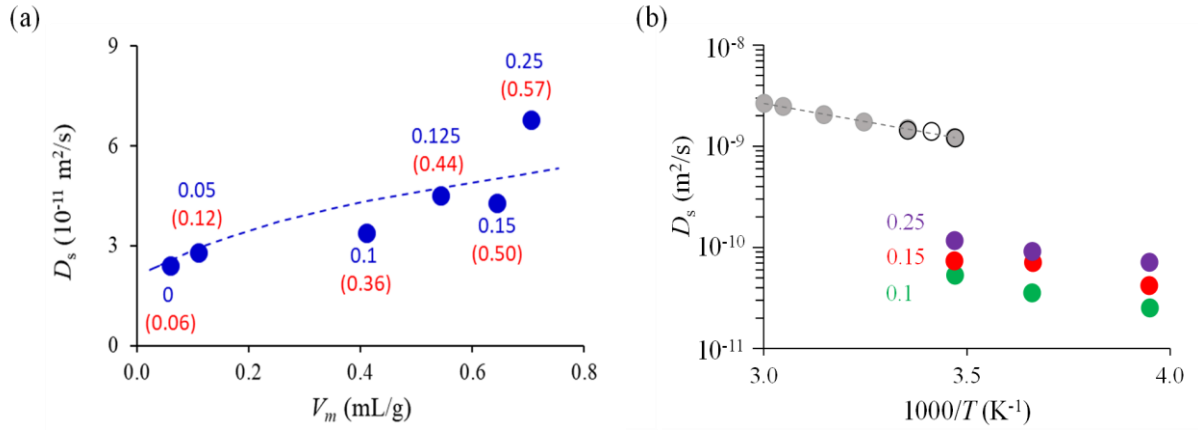

Fig. 4. (a) Self-diffusivity D_s as a function of the mesoporous volume V_m for cyclohexane adsorbed at T = -20 °C with Δ = 10 ms in mesoporous FAU. For each system, the whole porosity (micro- and mesoporosity) is filled. The dashed line is a fit against the fast exchange model (*see text*). The number in blue text close to each data point indicates the NaOH/Si molar ratio used to obtain the mesoporous FAU sample, while the red text in brackets indicates the corresponding mesoporosity ε (see table 1). (b) Effect of temperature on the self-diffusivity, D_s, as measured by PFG NMR for cyclohexane that fully fills the porosity of mesoporous FAU: (green circles) NaOH/Si = 0.1, (red circles) NaOH/Si = 0.15, and (purple circles) NaOH/Si = 0.25. The grey and white circles are the self-diffusivity for bulk cyclohexane (where the grey data are from this work, the white circles are taken from the literature).

Fig. 4(b) compares the temperature dependence of the self-diffusion coefficient for bulk cyclohexane and cyclohexane confined within three mesoporous FAU samples. All data follow nicely the expected Arrhenius behavior where the self-diffusion coefficients D_s vary exponentially with temperature T as $D_s = D_s^0 \times \exp(-E_{\text{act}}/k_{\text{B}}T)$. The pre-exponential factor D_s^0 is the high temperature self-diffusion coefficient that would be unaffected by the activation energy for molecular diffusion E_{act} (k_{B} is Boltzmann constant). D_s^0 is directly proportional to the molecular rate (frequency) with which molecules attempt to diffuse from one site to another. As expected, D_s^0 is strongly affected by confinement; while $D_s^0 \sim 4\times10^{-7}$

m^2/s for bulk cyclohexane, its value drops by 1 or 2 orders of magnitude upon confinement within the hierarchical zeolites; D_S^0 ~ 0.4–1×10^{-8} m^2/s. On the other hand, E_{act} is weakly or at least less dependent on confinement; E_{act} ~ 14 kJ/mol for bulk cyclohexane while E_{act} ~ 8–13 kJ/mol under confinement. This suggests that the molecular mechanism involved in diffusion is somewhat similar to its bulk counterpart. Overall, the different results above suggest that despite strong confinement within the porosity of the samples, the slower diffusion for confined cyclohexane arises from a lower diffusion rate D_S^0 (i.e. site accessibility through brownian diffusion jumps) rather than from confinement effects on the activation energy (which is slightly lower upon confinement).

4.2. Partial pore filling

As described in the previous section, the data for confined cyclohexane when the whole porosity –i.e. microporosity + mesoporosity – is filled, leads to a rather intuitive behavior. In contrast, the results obtained for partially filled hierarchical zeolites remain puzzling by many aspects. Fig. 5a shows the spin echo attenuation curve for cyclohexane adsorbed in a mesoporous FAU (the NaOH/Si molar ratio is 0.1 (V_μ = 0.22 mL/g, V_m = 0.41 mL/g, V_{tot} = 0.63 mL/g; see table 1 for further details). Data are shown for different filling ratios ranging from α = 40–100% of the total pore volume. The first experiments were performed at α = 100% and 40%, respectively, by applying a much larger range of magnetic field gradient pulses [$(\delta g\gamma)^2\Delta$ values] to obtain the diffusion characteristics for the boundary cases. For a sample with intermediate filling fraction (such as 60%), owing to the long data acquisition time required for a good signal to noise ratio in the PFG NMR experiments performed on our samples, the $(\delta g\gamma)^2\Delta$ range was restricted to a region where the slowest diffusing molecular population was expected, which is most relevant for this study. Thus, the fast initial attenuation has not been explored for the case of α = 60%. For α = 40% and 60%, corresponding to pores filled with 0.25 and 0.38 mL/g of cyclohexane, respectively, most molecules are within the microporosity with smaller and larger amounts of cyclohexane adsorbed at the mesopore surface, respectively. Strikingly, upon decreasing the filling fraction from 100% to 40%, the self-diffusion coefficient D_S increases. This result can be rationalized by considering diffusion (relocation) through the gas phase. In more detail, for partial filling fractions, some molecules diffuse not only through the microporosity and the mesopore surface but also through the gas phase in the mesoporosity. As the filling fraction decreases,

such a gas phase contribution necessarily increases as an increasing fraction of molecules within the microporosity or adsorbed film in the mesoporosity are in contact with the empty mesoporosity. In turn, this implies that upon decreasing the filling fraction, the overall contribution of the gas phase diffusion to the effective diffusivity D_s increases – in qualitative agreement with the data shown in Fig. 5(a). For α = 40% and 60%, the available volumes for the gas phase in mesopores correspond to 0.38 mL/g and 0.25 mL/g, respectively. It can be observed that the self-diffusion coefficient increases proportionately with the volume available for the gas phase.

While the reasoning above requires further study to be corroborated, it is supported by the three following results. First, in all cases, the self-diffusion coefficient, D_s, for the partially filled mesoporous FAU is higher than the value observed for the completely filled material. Considering that both D_s in the microporosity and in the adsorbed film are lower than in the mesoporosity (because of increasing confinement effect for the former and decaying fluid/surface interaction with film thickness for the latter), the overall diffusivity, D_s, should increase with increasing filling fraction if no gas phase contribution were to be considered. Second, considering the two datasets for partially filled samples, it can be assumed that in the thicker adsorbed film a smaller fraction of molecules relocate through the gas phase as the volume accessible to the gas is smaller. Such a thickness dependence of the gas phase diffusivity contribution explains why the measured self-diffusivity for partially filled samples in Fig. 5(a) decreases upon increasing the loading. The NMR signal attenuation represents the effective diffusivity of the entire adsorbed phase present in the micro- and mesoporous domains put together. Depending on the $(\delta g\gamma)^2\Delta$ range chosen (the larger the value, the smaller the length scale of diffusion probed, and vice versa), we go from a primarily gas phase diffusion dominated regime in the mesoporosity (low $(\delta g\gamma)^2\Delta$ range; rapid attenuation) to a regime dominated by molecular diffusion in the faujasite network (high $(\delta g\gamma)^2\Delta$ range; slow attenuation). Here we focus on the slowest diffusing molecules that are typically concentrated in the microporosity, and best represented by the slowest attenuation rate sustained over the broadest $(\delta g\gamma)^2\Delta$ range (Fig. 5(a)). A rough estimation of the fraction, *x*, of such population could be made by simply extrapolating this linear region of the NMR attenuation in Fig. 5(a) to $(\delta g\gamma)^2\Delta$ = 0.[19] In other words, the other 1-*x* molecule fraction diffuses too fast to contribute to the corresponding self-diffusivity (their self-diffusion is fast so that their contribution to the spin echo attenuation is located in a much smaller field

gradient range). While x ~ 0.5–0.6 for the completely filled hierarchical zeolite, this value drops to approximately 0.2 and 0.06 for the 60% and 40% filling fractions, respectively. This large decrease in the fraction of molecules contributing to the self-diffusion is consistent with the picture proposed above. In more detail, upon decreasing the filling fraction, more and more molecules explore the gas-filled porosity with only a limited contribution returning (i.e., relocating) within the same zeolite or adsorbed film domain over the typical observation time Δ.

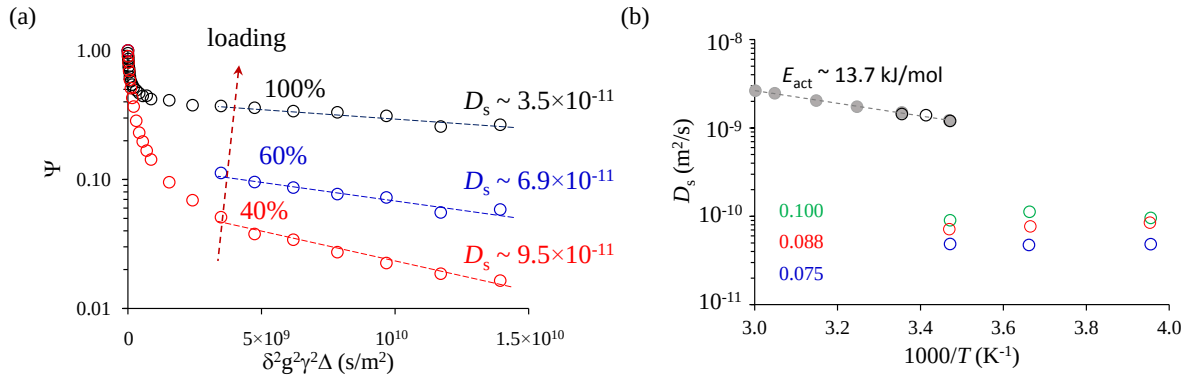

Fig. 5. (a) Attenuation Ψ of the spin echo signal at -20 °C for Δ = 10 ms as a function of the gradient strength, g, measured by PFG NMR for cyclohexane adsorbed in a mesoporous FAU (the NaOH/Si molar ratio is 0.1). The porosity is partially or totally filled with a filling ratio increasing from 40–100% (a loading of 40% means that only the microporosity is filled with some adsorbed molecules at the mesopore surface, while a loading of 100% means that both the microporosity and mesoporosity are filled with cyclohexane). These measurements were performed for an observation time Δ = 10 ms. The graph also reports the self-diffusivity D_s obtained from such attenuation curves. (b) Effect of temperature on the self-diffusivity, D_s, as measured by PFG NMR for cyclohexane adsorbed in mesoporous FAU: (green circles) NaOH/Si = 0.1, (red circles) NaOH/Si = 0.088, and (blue circles) NaOH/Si = 0.075. The grey and white circles are the self-diffusivity for bulk cyclohexane. All data for confined cyclohexane, which were taken for T = -20, 0, and 15°C, correspond to a loading where the microporosity is completely filled with some adsorbed molecules at the mesopore surface (filling ratio 40%).

To shed more light on the diffusion mechanisms in partially filled hierarchical zeolites, the temperature was varied in the range from -20 to +15 °C. The corresponding data are shown in Fig. 5(b) where we compare the results for bulk cyclohexane and cyclohexane confined in

different hierarchical zeolites. For the latter, the filling fraction was set to a value (40% of V_{tot}) where most molecules are located within the microporosity with a small amount of molecules adsorbed at the mesopore surface. In contrast to the data obtained for completely filled samples, these data show a non-Arrhenius behavior as D_s remains nearly constant upon increasing temperature. In an attempt to rationalize this result, we consider a possible effect of population redistribution upon changing the temperature. Indeed, the filling fraction, $f \sim 40\%$ – chosen here as it corresponds to a filling where most molecules only fill the microporosity – was defined from an adsorption isotherm obtained at room temperature. To verify the role of temperature, we focus on the cyclohexane adsorption isotherms measured at different temperatures for one of the mesoporous FAU (NaOH/Si = 0.125), as shown in Fig. 6(a). Such data are typical of adsorption isotherms for fluids in microporous/mesoporous samples. The hysteresis loops observed in the cyclohexane adsorption isotherms in the mesoporous FAU arises from capillary condensation in the mesoporosity. Indeed, as for N_2 adsorption at 77 K, cyclohexane in the mesoporosity also displays irreversibility upon adsorption/desorption.[33,34] In contrast, in the zeolite microporosity, these hysteresis loops are not observed since capillary condensation in such extreme confinement is replaced by a continuous, reversible pore filling.[35,36] As shown in Fig. 6(a), we also use Polanyi's model which allows predicting the adsorption isotherm at a given temperature, *T'*, from experimental data at a close but different temperature, *T*.[37,38] Polanyi's model can be simply derived in the framework of the Frenkel-Halsey-Hill theory[39,40,41] which postulates that the chemical potential μ of the adsorbed phase at a temperature *T* can be expressed as the chemical potential μ_0 of the liquid phase at saturation (i.e. at the saturating vapor pressure P_0 at the temperature *T*) corrected for the interaction potential *U* between the adsorbed phase and solid surface, $\mu(T) = \mu_0(T) - U$. This pertubative theory therefore assumes that the adsorbed phase is identical to the bulk liquid but affected by an energy term arising from the interactions with the solid surface. At thermodynamic equilibrium, the chemical potentials of the gas and adsorbed phase are equal so that the above equation can be written as $k_B T \ln P/P_0 = -U$ (we checked that the gas behaves ideally at all temperatures considered here so that the fugacity *f* can be replaced by the pressure *P*). This equation is identical to the hypothesis formulated in Polanyi's model, which assumes that the chemical potential leading to an adsorbed volume Nv (N is the adsorbed amount while v is the molar volume of the adsorbed phase assumed to be equal to its bulk liquid counterpart) is independent of temperature:

$$Nv = \phi\left[k_B T \ln \frac{P}{P_0(T)}\right] \qquad (3)$$

, where $\phi[x]$ is a function of the variable $x = k_B T \ln P/P_0(T)$ that is characteristic of the fluid/solid couple considered. Eq. (3) is very important as it allows predicting the adsorbed amount N as a function of pressure P (in fact, more rigorously, as a function of chemical potential μ) at any temperature T' from the adsorption isotherm $N(T,P)$ at a reference temperature T. As shown in Fig. 6(a), the application of the Polanyi model to cyclohexane adsorption data in mesoporous FAU samples was found to reasonably describe the experimental data obtained at lower temperatures.

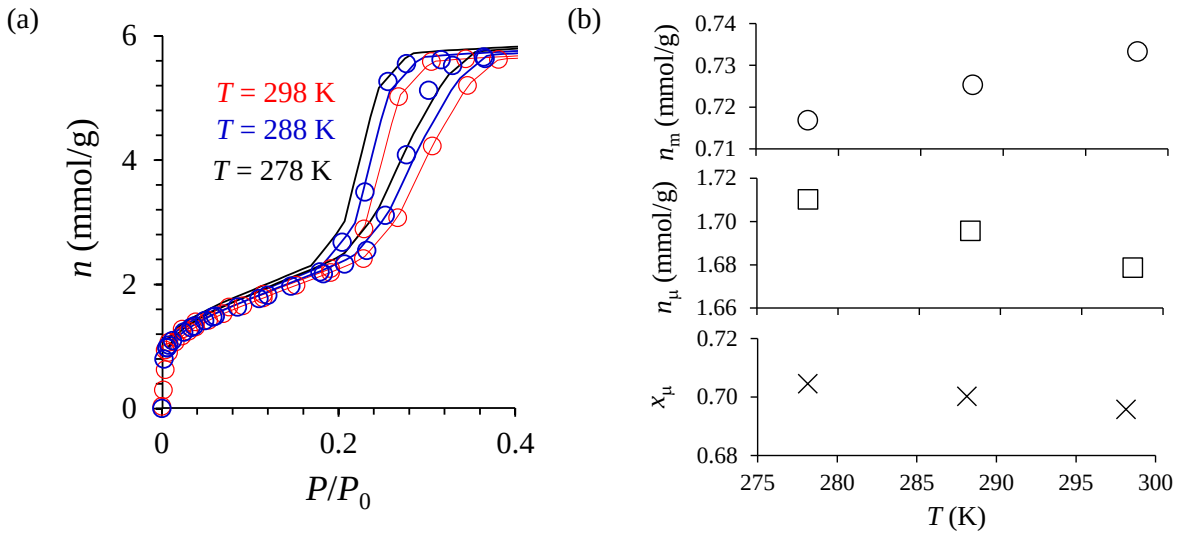

Fig. 6. (a) Cyclohexane adsorption isotherms at different temperatures in a mesoporous FAU (the NaOH/Si molar ratio is 0.125). The red, blue, and black colors correspond to T = 5, 15, and 25 °C, respectively. The symbols correspond to experimental measurements while the lines correspond to predictions using the Polanyi model applied to the experimental data obtained at 25°C (*see text*). (b) Cyclohexane adsorbed amount, n_m, in the mesopores (*top*, circles), n_μ, in the micropores (*middle*, squares) and fraction of molecules in the micropores, x_μ, for a porous volume filled at α = 40%.

Coming back to the interpretation of the diffusion results shown in Fig. 5(b) for different temperatures, the data obtained using Polanyi's model were used to estimate the amount of molecules in the micro- and mesoporosity as a function of T. The total number of moles of cyclohexane in the sample holder, N_T, at a pressure, P, and temperature, T, can be expressed as $N_T(P,T) = N_{m+\mu}(P,T) + N_g(P,T)$, where $N_{m+\mu}$ is the total number of moles in the meso- and micropores combined and N_g is the number of moles in the gas phase. By using the sample mass, m, the gas density $\rho_g(P,T) = P/RT$ (since we assume an ideal gas behavior), and the volume accessible to the gas phase, V_g, we can rewrite this equation as:

$$N_T(P,T) = m \times n_{m+\mu}(P,T) + V_g\, P/RT \qquad (4)$$

, where $n_{m+\mu}$ is the number of moles in the mesopores and micropores per g of sample.

As already mentioned, in this study, the pore loading at T = 25°C was chosen as 40% of the overall capacity so that the microporosity is ~100% filled while the mesopores are only covered by an adsorbed film. Such a loading corresponds to an adsorbed amount $n_{m+\mu}$ = 2.41 mmol/g obtained by fixing a gas pressure, $P = 0.2425P_0$ = 3115.4 Pa (since P_0 = 12847 Pa at T = 25°C). Using $V_g \sim 2\times10^{-6}$ m^3 and $m \sim 0.1$ g, Eq. (3) leads to $N_T \sim 0.265$ mmol. Since we decrease the temperature down to 15 and 5 °C while keeping N_T constant, we need to find the set [P, $n_{m+\mu}(P)$] that leads to the same N_T at each of these two temperatures. In practice, this is easily done since $n_{m+\mu}(P)$ can be predicted at each temperature from Eq. (4). Hence, we find the couple [P, $n_{m+\mu}(P)$] which satisfies Eq. (3) with N_T = 0.265 mmol. Once this is done, to determine n_m and n_μ at each temperature, we simply use the superimposition principle[10,42] that states that $n_{m+\mu}(P,T) = n_m(P,T) + n_\mu(P,T)$ (where all quantities are per g of mesoporous FAU sample). As shown in the example considered here, this is simply done by writing that the adsorption isotherm for the hierarchical zeolite is a linear combination of the adsorption isotherms – $n_\mu^{ref}(P,T)$ and $n_m^{ref}(P,T)$ – of the reference zeolite and the reference mesoporous sample (here a MCM-41 sample). In practice, this is done by fitting $n_{m+\mu}(P,T)$ against $\gamma_m n_m^{ref}(P,T) + \gamma_\mu n_\mu^{ref}(P,T)$, where γ_m and γ_μ are the weighing parameters (examples and details can be found in Refs. 10 and 42). Such fitting is limited to the low pressure range to avoid introducing non-physical effects arising from the differences in the sample intergranularity/external surface between the reference and hierarchical zeolites. Once the volume fractions γ_m and γ_μ have been determined for a given sample, they are obviously assumed to remain constant upon changing the temperature. This allows determining n_m and n_μ for T = 25, 15, and 5°C. As shown in Fig. 6(b), upon imposing $n_{m+\mu}$ = 2.41 mmol/g, we

found that n_μ decreases upon increasing T while n_m increases. While it is rather counterintuitive that n_m increases, we recall that the total system having a constant number of molecules includes a non-negligible gas phase; as a result, the increase in the number of molecules in the gas phase upon increasing T leads to a larger equilibrium pressure. The latter can partly counterbalance or even overbalance the decrease in the adsorbed amount due to increased thermal motion. Considering the molecules contained in the microporosity, n_μ, the ones adsorbed at the solid surface in the mesoporosity, n_m, and the gas phase in the mesoporosity, n_g, we find that the fraction of molecules adsorbed in the mesoporosity, x_m, increases while that in the microporosity, x_μ, decreases upon increasing T.

Quantitatively, as shown in Fig. 7, by assuming a fast diffusion regime where molecules explore both the micro- and mesoporosity, the estimated number of molecules in the gas phase, microporosity, and mesoporosity allows us to predict the effective diffusivity at each temperature using a simple linear combination rule: $D_s \sim x_m D_s^m + x_\mu D_s^\mu + x_g D_s^g$ (where D_s^m, D_s^μ, and D_s^g are the self-diffusivities in the mesoporosity, microporosity and gas phase, respectively). In what follows, we explain how D_s^m, D_s^μ, and D_s^g were estimated. In this figure, the two mesoporous FAU samples prepared with the molar ratios NaOH/Si = 0.125 and NaOH/Si = 0.075, respectively, were selected as they display mesoporous volumes in the high and low ranges, respectively (see Table 1 where the mesoporous volume is about twice larger for the mesoporous FAU sample prepared with NaOH/Si = 0.125).

Mesoporous diffusivity, D_s^m. Following the work by Mehlhorn et al.[43], the mesoporous diffusivity was taken as $D_s^m \sim 10^{-10}$ m^2/s; this value was estimated using a mesoporous zeolite material with zeolitic pores too small to accommodate cyclohexane so that its diffusivity was limited to the mesoporosity. This typical self-diffusivity is consistent with other experimental measurements on cyclohexane in silica nanopores, where D_s^m was found to be of the same order of magnitude.[44,45] Moreover, as expected for diffusivity in mesoporous domains, this value is about an order of magnitude smaller than the bulk self-diffusivity observed for cyclohexane under similar thermodynamic conditions, $D_s \sim 10^{-9}$ m^2/s. Moreover, it was checked that even if exact predictions for D_s depend on the specific values chosen for the mesoporous diffusivity, the conclusions below remain qualitatively valid. As for the

temperature dependence, D_s^m was assumed to follow an Arrhenius behavior with an activation energy similar to the bulk activation energy [E_a ~ 15 kJ/mol].

Microporous diffusivity D_s^μ. As for the microporosity diffusivity, it was taken as $D_s^\mu \sim 10^{-11}$ m^2/s as it corresponds to the limit observed from our experimental data in Fig. 4(a) when the mesoporous volume, V_m, becomes vanishingly small. As expected, this value obtained for FAU-Y samples is about an order of magnitude higher than measurements on FAU-X, $D_s^\mu \sim 5\times10^{-13} - 10^{-12}$ m^2/s, as a larger number of cations in FAU-X leads to strong steric effects and hence hindered diffusion.[46] As for the temperature dependence of these diffusivities, based on our experimental data shown in Fig. 4(b), D_s^μ was also modeled according to an Arrhenius law with E_{act} ~ 15 kJ/mol.

Gas diffusivity D_s^g. As the experimental temperatures considered here are much lower than the critical point of cyclohexane (T_c = 554 K), the gas phase in the mesoporosity can be treated as an ideal gas. Consequently, the self-diffusivity of the gas phase was assumed to correspond to Knudsen diffusivity at the corresponding temperature: $D_s^g = dv/3$ where $v = [8k_BT/\pi m]^{1/2}$ is the thermal velocity at the corresponding temperature T, while d ~ 4.5 nm is the mean mesopore diameter in which Knudsen diffusion occurs (m is the mass in kg of the cyclohexane molecule).

Before analyzing quantitatively our results, a few remarks are in order. First, on the one hand, the gas phase volume taken into account for the thermodynamic calculations (i.e. redistribution between microporosity, mesoporosity, and gas phase) corresponds to the whole gas phase contained in the macropores outside the solid sample as well as in the mesopores. On the other hand, when applying the fast diffusion model (i.e. effective diffusivity using a simple linear combination of the different porosities/contributions), we only take into consideration the gas phase contained in the mesoporosity. This difference is justified by the fact that gas diffusion in the macroporosity (outside the porous solid) diffuses extremely fast with a self-diffusion coefficient that is orders of magnitude faster than the gas diffusion in the mesoporosity; as a result, such very fast diffusion corresponds to the attenuation decay seen at small field gradients that do not contribute to the estimated diffusivity. As discussed in the

previous paragraph, we use Knudsen diffusion to describe gas diffusion in the mesoporosity. While this might correspond to a simplified description of complex diffusion in such situations (gas diffusing in mesopores, the surface of which is covered by an adsorbed film), it provides a more refined picture than ideal gas diffusion. In practice, the mesoporous diameter considered in these calculations corresponds to the nominal pore diameter, d = 4.5 nm, without correcting for the adsorbed film thickness, t, as the latter is assumed to be small (t < 1 nm << d). Coming back to our data, as shown in Fig. 7, even if the adsorbed amounts in the micro- and mesoporosity change by only a few percent when increasing the temperature, important changes are observed in the predicted effective self-diffusivity (with a noticeable non-Arrhenius behavior). When considering the linear rule, $D_s \sim x_m D_s^m + x_\mu D_s^\mu + x_g D_s^g$, D_s is found to increase with temperature in stark contrast with the experimental PFG NMR data shown in Fig. 5(b). Moreover, the predicted D_s is found to largely overestimate the experimental measurements. Such very fast effective diffusivities arise from the gas phase contribution, the diffusivity of which (~10^{-7} m^2/s) largely prevails over the diffusivity in the micro-and mesoporous phases (~10^{-11} m^2/s and ~10^{-10} m^2/s, respectively). Such analysis suggests that the experimental data cannot be rationalized by including the contribution from the gas phase diffusivity (even if Knudsen diffusion, which is slower than the ideal gas diffusivity, is considered for the gas confined in the mesoporosity). Fig. 7 also shows the predicted values when neglecting the gas phase contribution, i.e. $D_s \sim x'_m D_s^m + x'_\mu D_s^\mu$ (where the ' indicates that we only consider molecules in these two phases so that $x'_m + x'_\mu = 1$). As expected, for the two mesoporous FAU samples considered here (NaOH/Si = 0.075 and NaOH/Si = 0.125), it is found that the gas phase contribution largely impacts the predicted effective self-diffusivity. This result is further supported by the fact that the impact of such gas phase contribution is larger for the sample with larger mesoporosity (NaOH/Si = 0.125). Yet, like with the predictions accounting for the gas phase, it is found that the predicted diffusivities still overestimate the experimental values when the gas phase contribution is removed (even if overall the discrepancy between the predicted and observed diffusivities is much smaller).

Before continuing our analysis, a discussion on the need to include the gas phase contribution in the predicted diffusivity is in order. For partially filled pores (i.e. 40% filling), a gradually varying attenuation is observed in the attenuation curve until reaching attenuation corresponding to the slowest molecules at large field gradients. We expect the contribution of

the molecules in the gas phase to correspond to attenuation observed in the small field gradient range (and not just in the slowest part observed at high field gradients). However, while this analysis suggests that the gas phase contribution should not be included when predicting the effective diffusivity from the high field gradient, we have already pointed earlier different arguments showing that such fast diffusion does contribute. In fact, the gas phase contribution is non-trivial as the gradually changing attenuation curve reflects a gradient of molecular diffusivities with a non-negligible number of molecules in the microporosity and adsorbed film exploring some of the gas phase.

The analysis above suggests that accounting for populations in the micro- and mesoporosity as a function of temperature is not sufficient to capture the very weak temperature dependence of the effective diffusivity in partially loaded hierarchical samples. Due to the difficulty in assessing the exact contribution from the gas phase diffusivity, the combined dynamical/thermodynamic modeling used here is necessary but not sufficient to capture the effective self-diffusivity measured at various temperatures. While further experimental and theoretical work is needed to unravel the complex behavior observed for the effective diffusivity, the following interpretation provides a first qualitative picture. Careful analysis of the attenuation data leading to D_s shows that upon increasing T, the overall fraction of molecules to which the extracted self-diffusivity applies decreases from 10% down to 0.1%. This result can be explained as follows; with increasing T, there is an increasing amount of molecules that escape through the gas phase without relocating within the adsorbed or confined phase over the observation time, Δ. This implies that upon increasing T, the spin echo attenuation used to estimate D_s corresponds to an increasingly smaller number of molecules. In turn, this means that while the molecular population diffuses overall faster with increasing T, our measurements rely at each temperature on the slowest population contribution (the ones that do not diffuse too fast to contribute to the spin echo attenuation in the monitored field gradient range). At this stage, even if the non-trivial variations in the microporous, mesoporous, and gas phase contributions must be also taken into account, the last explanation above is sufficient to rationalize – at least qualitatively – the anomalous temperature dependence of the effective self-diffusivity in partially filled porous solids.

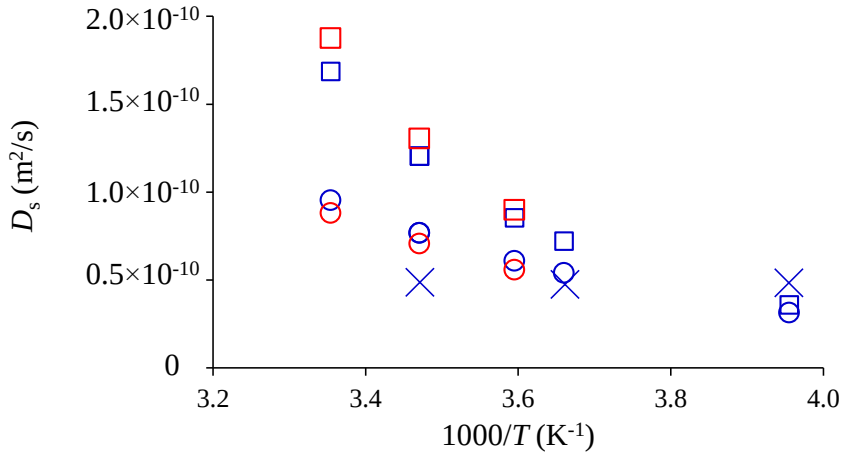

Fig. 7. Predicted and experimental **s**elf-diffusivity, D_s, as a function of temperature for the mesoporous FAU samples prepared with NaOH/Si = 0.125 (red data) and NaOH/Si = 0.075 (blue data). The open squares are obtained by considering the gas phase included in the mesoporosity while the open circles neglect such contribution. The crosses correspond to the experimental measurements for the mesoporous FAU prepared with NaOH/Si = 0.075 filled at 40% V_{tot} (*see text*).

5. DISCUSSION AND CONCLUSION

In this paper, the self-diffusion of cyclohexane in hierarchical zeolites combining the zeolite microporosity and an ordered mesoporosity consisting of cylindrical pores was investigated using PFG NMR. For samples exhibiting different mesoporous volumes, the effect of loading with both partially and totally filled porosities was studied as a function of temperature. For totally filled samples, the self-diffusion coefficient for cyclohexane can be easily rationalized as the data behave as expected. The self-diffusivity increases upon increasing the mesoporous volume within the hierarchical zeolite and follows an Arrhenius behavior with respect to temperature, with an activation energy that is smaller but close to its bulk counterpart. In contrast, cyclohexane in partially filled hierarchical zeolites shows an unexpected behavior as the self-diffusivity decreases upon increasing the loading and remains nearly constant (or even slightly decreases) upon increasing temperature. These results can be rationalized by taking into account the population redistribution between the microporosity, mesoporosity and gas phase, but also the effective fraction, *x*, of molecules that contribute to the spin echo attenuation probed in PFG NMR. In particular, considering that the fraction of molecules probed in PFG NMR applied to partially filled samples decrease upon increasing the

temperature, we propose here that such measurements could yield effective diffusivities with an anomalous temperature dependence.

Overall, even if the predictive power of the formal analysis performed here is limited, it sheds light on the complex diffusion mechanisms inside hierarchical nanoporous materials. In particular, while diffusion data are usually analyzed using effective models, we show here that a robust thermodynamic treatment is required to probe quantitatively the impact of gas phase diffusion. Moreover, while such contribution has a large impact on the predicted diffusivity, we also show that other factors must be taken into account, such as the nature of the molecular population being actually probed using PFG NMR experiments in specific conditions. While such effects are not relevant or minor for completely filled pores, they are key when considering partially filled pores. These results emphasize some of the difficulties encountered in using PFG NMR to estimate the self-diffusivity of gas probes in hierarchical porous samples. While the data for completely filled mesoporous zeolites are rather straightforward to analyze, the case of partially filled samples turns out to be quite complex. From a technical viewpoint, this inherent difficulty arises from the dual nature of the PFG NMR experiment itself. Indeed, in such experiments, one varies both the timescale and lengthscale over which the self-diffusivity is probed. While Δ sets the typical time, the field gradient imposes a characteristic length ξ. The choice made for these two parameters – which cannot be tuned to a very broad extent in any case – is critical as it restricts the time/length window being probed. In particular, the set of values $[\Delta, \xi]$ selects a specific subset of molecules being used to determine the self-diffusivity. While this is a well-known physical effect in PFG NMR, it highlights the need to span a range of conditions sufficiently broad in these experiments applied to hierarchical porous samples to obtain a clear and robust physical picture of self-diffusivity in such complex environments.

Supporting Information. The Supporting Information is available free of charge on the ACS Publications website at DOI: 10.1021/acs.langmuir.xxxxxxx. Additional data including spin echo attenuation curves with fits to obtain the different self-diffusion coefficients.

Acknowledgments. The authors thank TotalEnergies OneTech Belgium for financial support. We also acknowledge support from the French Research Agency (ANR TAMTAM 15-CE08-0008).We are very grateful to Dr. Dirk Mehlhorn for his contribution with NMR experiments and useful discussion.

REFERENCES

(1) Van Der Voort, P.; Leus, K.; De Canck, E. *Introduction to Porous Materials;* John Wiley & Sons: New Jersey, U.S., 2019.

(2) Van Donk, S.; Janssen, A. H.; Bitter, J. H.; de Jong, K. P. Generation, Characterization, and Impact of Mesopores in Zeolite Catalysts. *Catal. Rev. Sci. Eng*. **2003**, *45*, 297-31.

(3) Corma, A. From Microporous to Mesoporous Molecular Sieve Materials and Their Use in Catalysis. *Chem. Rev.* **1997**, *97*, 2373–2420.

(4) Ivanova, I. I.; Knyazeva, E. E. Micro–Mesoporous Materials obtained by Zeolite Recrystallization: Synthesis, Characterization and Catalytic Applications. *Chem. Soc. Rev*. **2013**, *42*, 3671-3688.

(5) Perez-Ramirez, J.; Mitchell, S.; Verboekend, D.; Milina, M.; Michels, N. L.; Krumeich, F.; Marti, N.; Erdmann, M. Expanding the Horizons of Hierarchical Zeolites: Beyond Laboratory Curiosity towards Industrial Realization. *ChemCatChem* **2011**, *3*, 1731-1734.

(6) Mitchell, S.; Michels, N-L.; Kunze, K.; Perez-Ramirez, J. Visualization of Hierarchically Structured Zeolite Bodies from Macro to Nano Length Scales. *Nat. Chem*. **2012**, *4*, 825 – 831.

(7) Carvalho-Filho, A.F.; Alcântara, A.C.; Paiva, A.E.; Passinho-Silva, J.J.; Perez-Carvajal, J.; Rojas, A. Thermal kinetics on adsorption heat transformation based on activated biocarbon and ethanol as working pairs. *Mater. Lett.* **2022**, *311*, 131622.

(8) Jedli, H.; Almoneef, M.M.; Mbarek, M.; Jbara, A.; Slimi, K. Adsorption of CO_2 onto zeolite ZSM-5: Kinetic, equilibrium and thermodynamic studies. *Fuel* **2022**, *321*, 124097.

(9) Coasne, B. Multiscale Adsorption and Transport in Hierarchical Porous Materials. *New J. Chem.* **2016**, *40*, 4078-4094.

(10) Coasne, B.; Galarneau, A.; Gerardin, C.; Fajula, F.; Villemot, F. Molecular Simulation of Adsorption and Transport in Hierarchical Porous Materials. *Langmuir* **2013**, *29*, 7864.

(11) Jobic, H.; Fitch, A. N.; Combet, J. Diffusion of Benzene in NaX and NaY Zeolites Studied by Quasi-Elastic Neutron Scattering. *J. Phys. Chem. B* **2000**, *104*, 8491-8497.

(12) Jobic, H.; Theodorou, D. N. Quasi-Elastic Neutron Scattering and Molecular Dynamics Simulation as Complementary Techniques for Studying Diffusion in Zeolites. *Microp. Mesop. Mater*. **2007**, *102*, 21-50.

(13) Kimmich, R. *Spin-Lattice Relaxation in NMR, Tomography, Diffusometry, Relaxometry;* Springer-Verlag: Berlin Heidelberg, 1997; pp 102–115.

(14) Chemmi, H.; Petit, D.; Levitz, P.; Denoyel, R., Galarneau, A.; Korb, J. P. Noninvasive Experimental Evidence of the Linear Pore Size Dependence of Water Diffusion in Nanoconfinement. *J. Phys. Chem. Lett.* **2016**, *7*, 393−398.

(15) Levitz, P. Probing Interfacial Dynamics of Water Confined in Nanoporous Systems by NMRD. *Mol. Phys.* **2019**, *117*, 952–959.

(16) Karger, J.; Valiullin, R. Mass Transfer in Mesoporous Materials: The Benefit of Microscopic Diffusion Measurement. *Chem. Soc. Rev.* **2013**, *42*, 4172-4197.

(17) Schneider, D.; Mehlhorn, D.; Zeigermann, P.; Karger, J.; Valiullin, R. Transport Properties of Hierarchical Micro-Mesoporous Materials. *Chem. Soc. Rev.* **2016**, *45*, 3439-3467.

(18) Galarneau, A.; Guenneau, F.; Gedeon, A.; Mereib, D.; Rodriguez, J.; Fajula, F.; Coasne, B. Probing Interconnectivity in Hierarchical Microporous/Mesoporous Materials Using Adsorption and Nuclear Magnetic Resonance Diffusion. *J. Phys. Chem. C* **2016**, *120*, 1562-1569.

(19) Karger, J.; Ruthven, D. M.; Theodorou, D. N. *Diffusion in Nanoporous Materials;* John Wiley & Sons: Weinheim, Germany, 2012.

(20) Falk, K.; Coasne, B.; Pellenq, R.; Ulm, F. –J.; Bocquet, L. Subcontinuum Mass Transport of Condensed Hydrocarbons in Nanoporous Media. *Nature Comm.* **2015**, *6*, 6949.

(21) Mehlhorn, D.; Valiullin, R.; Kärger, J.; Schumann, K.; Brandt, A.; Unger, B. Transport Enhancement in Binderless Zeolite X- and A-type Molecular Sieves Revealed by PFG NMR Diffusometry. *Microp. Mesop. Mater*. **2014**, *188*, 126-132.

(22) Martin, T.; Galarneau, A.; Di Renzo, F.; Fajula, F., Plee, D. Morphological Control of MCM-41 by Pseudomorphic Synthesis. *Ang. Chem. Int. Ed.* **2002**, *41*, 2590-2592.

(23) Adem, Z.; Guenneau, F.; Springuel-Huet, M. A.; Gedeon, A.; Iapichella, J.; Cacciaguerra, T.; Galarneau, A. Diffusion Properties of Hexane in Pseudomorphic MCM-41 Mesoporous Silicas Explored by Pulsed Field Gradient NMR. *J. Phys. Chem. C* **2012**, *116*, 13749-13759.

(24) Mehlhorn, D.; Rodriguez, J.; Cacciaguerra, T.; Radu-Dorin, A.; Guenneau, F.; Gedeon, A.; Coasne, B.; Thommes, M.; Minoux, D.; Aquino, C.; Dath, J. P.; Fajula, F.; Galarneau, A. Revelation on the Complex Nature of Mesoporous FAU-Y Zeolites. *Langmuir* **2018**, *34*, 11414.

(25) Galarneau, A.; Desplantier, D.; Dutartre, R.: Di Renzo, F. Micelle-Templated Silicates as a Test Bed for Methods of Mesopore Size Evaluation. *Microp. Mesop. Mater.* **1999**, *27*, 297.

(26) Desmurs, L.; Galarneau, A.; Cammarano, C.: Hulea, V.; Vaulot, C.; Nouali, H.; Lebeau, B.; Daou, T. J.; Vieira Soares, C.; Maurin, G.; Haranczyk, M.; Batonneau-Gener, I.; Sachse, A. Determination of Microporous and Mesoporous Surface Areas and Volumes of Mesoporous Zeolites by Corrected t-Plot Analysis. *ChemNanoMat* **2022**, e202200051.

(27) Cotts, R. M.; Hoch, M. J. R.; Sun, T.; Markert, J. T. Pulsed field gradient stimulated echo methods for improved NMR diffusion measurements in heterogeneous systems. *J. Magn. Reson.* **1989**, 83, 252-266.

(28) Galarneau, A.; Villemot, F.; Rodriguez, J.; Fajula, F.; Coasne, B. Validity of the t-plot Method to Assess Microporosity in Hierarchical Micro/Mesoporous Materials. *Langmuir* **2014**, *30*, 13266.

(29) Galarneau, A.; Mehlhorn, D.; Guenneau, F.; Coasne, B.; Villemot, F.; Minoux, D.; Aquino, C.; Dath, J. P. Specific Surface Area Determination of Microporous/Mesoporous Materials: the Case of Mesoporous FAU-Y Zeolites. *Langmuir* **2018**, *34*, 14134.

(30) Reich, S. J.; Svidrytski, A.; Hlushkou, D.; Stoeckel, D.; Kübel, C.; Höltzel, A.; Tallarek, U. Hindrance factor expression for diffusion in random mesoporous adsorbents obtained from pore-scale simulations in physical reconstructions. *Ind. Eng. Chem. Res.* **2018**, *57*, 3031-3042.

(31) Zeigermann, P.; Kärger, J.; Valiullin, R. Diffusion in microporous materials with embedded mesoporosities. *Microp. Mesop. Mater.* **2013**, *178*, 84-89.

(32) Zeigermann, P.; Naumov, S.; Mascotto, S.; Kärger, J.; Smarsly, B. M.; Valiullin, R. Diffusion in Hierarchical Mesoporous Materials: Applicability and Generalization of the Fast-Exchange Diffusion Model. *Langmuir* **2012**, 28, 3621-3632.

(33) Monson, P. A. Understanding adsorption/desorption hysteresis for fluids in mesoporous materials using simple molecular models and classical density functional theory. *Micropor. Mesopor. Mat.* **2012**, *160*, 47-66.

(34) Coasne, B. ; Galarneau, A.; Pellenq, R. J. M.; Di Renzo, F. Adsorption, intrusion and freezing in porous silica: the view from the nanoscale. *Chem. Soc. Rev.* **2013**, *42*, 4141-4171.

(35) Deroche, I.; Daou, T.J.; Picard, C.; Coasne, B. Reminiscent capillarity in subnanopores. Nat. Commun. **2019**, *10*, 1-10.

(36) Coasne, B.; Gubbins, K. E.; Pellenq, R. J. M. Temperature effect on adsorption/desorption isotherms for a simple fluid confined within various nanopores. *Adsorption* **2005**, *11*, 289-294.

(37) Rouquerol, J.; Rouquerol, F.; Llewellyn, P.; Maurin, G.; Sing, K. S. W. *Adsorption by Powders and Porous Solids: Principles, Methodology and Applications: Second Edition;* Academic Press, Elsevier: Oxford, U.K., 2013.

(38) Neimark, A. V.; Grenev, I. Adsorption-Induced Deformation of Microporous Solids: A New Insight from a Century-Old Theory. *J. Phys. Chem. C* **2020**, *124*, 749-755.

(39) Steele, W. A. *The Interaction of Gazes with Solid Surfaces;* Pergamon Press: Oxford, 1974.

(40) Coasne, B.; Grosman, A.; Ortega, C.; Pellenq, R. J. M. Physisorption in Nanopores of Various Sizes and Shapes: A Grand Canonical Monte Carlo Study. *Stud. Surf. Sci. Catal.* **2002**, *144*, 35-42.

(41) Coasne, B.; Pellenq, R. J. M. Grand Canonical Monte Carlo Simulation of Argon Adsorption at the Surface of Silica Nanopores: Effect of Pore Size, Pore Morphology and Surface Roughness. *J. Chem. Phys.* **2004**, *120*, 2913-2922.

(42) Deliere, L.; Villemot, F.; Farrusseng, D.; Galarneau, A.; Topin, S.; Coasne, B. Adsorption in Heterogeneous Microporous Materials. *Microp. Mesop. Mater.* **2016**, *229*, 145-154.

(43) Mehlhorn, D.; Valiullin, R.; Karger, J.; Cho, K.; Ryoo, R. Exploring the Hierarchy of Transport Phenomena in Hierarchical Pore Systems by NMR Diffusion Measurement. *Microp. Mesop. Mater.* **2012**, *164*, 273-279.

(44) Gjerdaker, L.; Aksnes, D. W.; Sorland, G. H.; Stocker, M. Relaxation and Diffusion Studies of Cyclohexane Confined in MCM-41 by NMR. *Microp. Mesop. Mater.* **2001**, *42*, 89-96.

(45) Aksnes, D. W.; Forland, K.; Stocker, M. 1H NMR Relaxation and Diffusion Studies of Cyclohexane and Cyclopentane Confined in MCM-41. *Microp. Mesop. Mater.* **2005**, *77*, 79-87.

(46) Mehlhorn, D.; Inayat, A., Schwieger, W.; Valiullin, R.; Karger, J. Probing Mass Transfer in Mesoporous Faujasite-Type Zeolite Nanosheet Assemblies. *ChemPhysChem* **2014**, *15*, 1681-1686.